Journal of Applied Electrochemistry (2007) 37:241–248
DOI 10.1007/s10800-006-9247-3

Electrochemical dissolution and passivation of nickel powder randomly dispersed in a graphite + polypropylene matrix

J. GREGORI[1], J.J. GARCÍA-JAREÑO[1], F. NEGRETE[1], M.P. PEÑA[1], C. SANZ[2], J. SUBIELA[1] and F. VICENTE[1,*]
[1]*Laboratory of Electrochemistry, Faculty of Chemistry, University of València, C/Dr. Moliner 50, 46100, Burjassot, Spain*
[2]*Technological Institute of Plastics (AIMPLAS), València Parc Tecnològic, C/ Gustave Eiffel 4, 46980, Paterna, Spain*
*(*author for correspondence, tel.: + 34-963543022, fax: + 34-963544564, e-mail: Francisco.Vicente@uv.es)*

Received 30 September 2005; accepted in revised form 15 September 2006

Key words: anodic dissolution, anodic Passivation, composite, graphite, nickel, CPE

Abstract

Nickel powder (10% in weight) randomly dispersed in a graphite (40%) + polypropylene (50%) matrix was studied as a composite electrode in a sulphuric-sulphate acid medium by means of voltammetry and Electrochemical Impedance Spectroscopy (EIS). Under voltammetric conditions, this thermoplastic material shows an electrochemical behaviour similar to nickel metal. However, under EIS measurement conditions the electrodissolution behaviour of the nickel powder is partially limited by the diffusion of the anions in the electrolyte in order to electroneutralize the excess of electrogenerated positive charge. The low frequency range of the measured impedance spectra can be interpreted as a parallel arrangement of a capacitive and a Warburg impedance, instead of a CPE element initially considered in the fitting. Values for CPE exponents lower than 0.85 are interpreted as a competition between a capacitive/transport contribution to the overall impedance response.

1. Introduction

From a technological point of view, nickel has great importance because of its use in rechargeable alkaline batteries [1], cathodes in fuel cells [2] and electrocatalysts for oxygen evolution [3]. Moreover, nickel is an element included in many alloys to increase their corrosion resistance [4–6]. Nickel has been the subject of many electrochemical studies regarding electrodissolution and passivation processes [7–11]. Nickel electrodissolution in acid medium takes place by two single electron transfer steps followed by a transport step [9–12]. Under voltammetric conditions, the appearance of one or two anodic peaks defines the active anodic dissolution/passive transition of nickel in acid media [8–11]. The same feature is also observed for a nickel powder randomly dispersed in a polymeric matrix [8].

Composite materials prepared by means of the dispersion of conducting particles in a polymeric material have become increasingly important in electronic industries such as antistatic, electromagnetic and radio frequency interference shielding, and for magnetic tapes [13, 14]. These materials have been studied for a wide variety of applications: from electrochemical detectors to biosensors [15–17]. Conducting particles + polymer composite materials are widely used in industry in low density metal structures and also as negative electrode materials in batteries [18]. From a fundamental point of view, the electrochemical behaviour and the preparation of these materials show interesting theoretical and experimental features [17, 19–27]. In general, graphite improves the electrical and other physical properties of the plastic component of these composites. It can be considered, in such cases, that the surface nickel particles act as a multi micro-electrode configuration [26].

The aim of this work is to study the electrochemical anodic dissolution of a nickel powder dispersed in a graphite + polymer composite matrix, since it is expected that the metal phase of the material determines its electrochemical behaviour. For that purpose, cyclic voltammetry experiments and EIS measurements were performed in order to compare the results for the anodic dissolution process of this system with the better known behaviour for a nickel electrode, since this composite material shows interesting thermoplastic properties and a low relative density when compared with nickel. Moreover, the passive state in acid medium was also studied because of the great tendency of self-passivation of nickel even in acid media and the technological importance of the passive nickel system.

2. Experimental procedure and materials

Conductivity measurements were carried out on different composite samples. These composite samples were made from a polypropylene (PP) + graphite matrix and different metal powders as fillers: Zn (Merck), Al (Merck) and Ni (Merck). The average diameter for graphite particles was 15 μm. To obtain the best distributive and dispersive effect, mixtures were made in two steps: a twin screw co-rotative extruder (Werner & Pfleiderer, ZSK 25) was used to improve the distributive effect in the mixture, and a Roll Mix mixer (Collin Gmbh) was used to improve the dispersive effect. A Platen Press equipment (Collin Gmbh) was finally used in order to obtain test samples (0.4 cm of width) with the following proportions in weight: 50% PP : 40% graphite : 10% metal powder.

Conductivity measurements were carried out with a Phillips PM 6304 LCR Metter. Electrical contacts were made with two nickel sheets (8.2 cm^2 of area) connected to copper wires and symmetrically disposed in parallel on each side of the composite samples. Impedance modulus, $|Z|$, and phase angle, Φ, values were measured at different applied potentials $E = 0$ V and $E = 2$ V, respectively. Sinusoidal potential variations with different potential amplitudes were superimposed, $\Delta E^{Low} = \pm 50$ mV, $\Delta E^{Normal} = \pm 1$ V and $\Delta E^{High} = \pm 2$ V, and frequencies ranging from $f = 100$ Hz–10^5 Hz. Before each experiment, both composite and nickel sheet surfaces were polished. Also conductivity measurements were carried out in a 50% PP : 50% graphite composite following the same procedure described above.

All the electrochemical experiments were carried out in a typical three electrode cell. The potential was measured versus the Ag/AgCl/KCl (sat.) or the Hg/$HgSO_4$/KSO_4 (sat) reference electrodes. A platinum grid was used as an auxiliary electrode. Solutions were prepared from K_2SO_4 (Probus, a.g.), H_2SO_4 (Merk, a.g.), with distilled and double deionised water (MilliQ). The geometrical area of the composite electrodes was 0.59 cm^2. In the case of electrochemical measurements, working electrodes were made from nickel powder (10% in weight) randomly dispersed in a graphite + polymer composite matrix. The average diameter of nickel particles was 5 μm. Also working electrodes made from a nickel sheet (99.9%, Johnson&Matthey) were used for comparison (geometrical are of 0.5 cm^2).

For impedance measurements the potential was controlled with a Potentiostat-Galvanostat 273A EG&G PAR and the impedance spectra were recorded with the aid of a Lock-in Amplifier 5210 EG&G PAR. The stabilization potential E_0 was applied for 60 min before recording each impedance spectrum. The stabilization potential represents the potential at which the corresponding electrochemical impedance spectrum was recorded after a steady state was reached. The impedance measurements were carried out in the frequency range [10^5, 5×10^{-2}] Hz and the amplitude of the harmonic potential perturbation was 5 mV *r.m.s*. The fitting of experimental impedance data to the proposed equivalent circuit was carried out by means of a non-linear least squares procedure based on the Marquardt algorithm for function optimization [28].

Voltammetric experiments at a scan rate of 0.5 mV s^{-1} were carried out in the [−0.70, 0.85] V vs Ag/AgCl/KCl (sat.) potential window. The potential was controlled with a Potentiostat-Galvanostat 273A EG&G PAR. Successive voltammetric experiments at 20 mV s^{-1} and single voltammograms at scan rates 1, 5, 10, 20, 40, 60, 80, 100, 150, 200 mV s^{-1} were performed by using a potentiostat (Wenking HP88). In this case potential and current values were measured by means of a Keithley 2700 multimeter. In both cases the potential window was [−1.7, 0.2] V vs Hg/$HgSO_4$/KSO_4 (sat).

Unless indicated otherwise solutions were deaerated by bubbling Ar (Air Liquide) for 5 min before starting the experiments. All the measurements were performed in an inert atmosphere, in still electrolyte conditions and constant and controlled temperature $T = 298$ K.

3. Results and discussion

3.1. *Conductivity of composite materials*

In all the analyzed composite samples the graphite content was greater than that required to overcome the first percolation threshold of the polymer + graphite binary system [21, 29–31]. The presence of metal powder in the matrix causes an increase in the system conductivity. Composite resistivity values can be calculated from $|Z|$ and Φ measurements (see Table 1). For the 50% PP : 50% graphite composite the calculated resistivity was 356 Ω cm, whereas for the composite filled with metal powders this value was at around 60 Ω cm in all cases. It is evident that the addition of metal powder to the polymer + graphite matrix considerably increases the conductivity of the material. As seen in Table 1, the nickel filled composite is the most conductive material, followed by the zinc filled and finally the aluminium filled.

3.2. *Cyclic voltammetry*

The voltammogram recorded at a low scan rate of 0.5 mV s^{-1} for the 50% PP: 40% graphite : 10% Ni powder composite electrode is represented in Figure 1 in the form of a ln i vs E plot.

Table 1. Impedance modulus, $|Z|$, phase angle, Φ, and calculated resistivity, ρ for the different composite samples. $E = 2$ V, $\Delta E = \pm 2$ V, $f = 100$ kHz

	PC	PCZn	PCNi	PCAl
$\|Z\|$/Ω	17	3	3	3
Φ/degree	2	14	15	10
ρ/Ω cm^{-1}	355	63	59	67

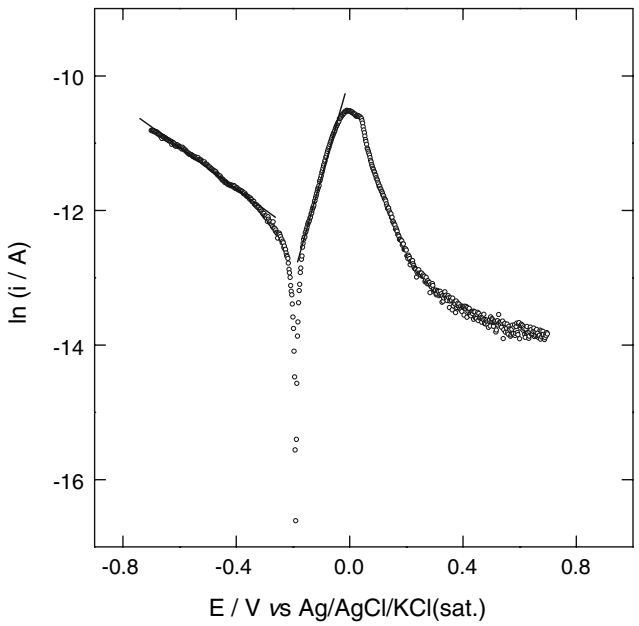

Fig. 1. Voltammetric curve for nickel powder randomly dispersed on a graphite + polypropylene matrix. Scan rate 0.5 mV s^{-1}, [−0.7, 0.85] V, 0.245 M K_2SO_4, 0.005 M H_2SO_4, pH = 2.7, T = 298 K. All the potentials are referred to the Ag/AgCl/KCl (sat.) reference electrode.

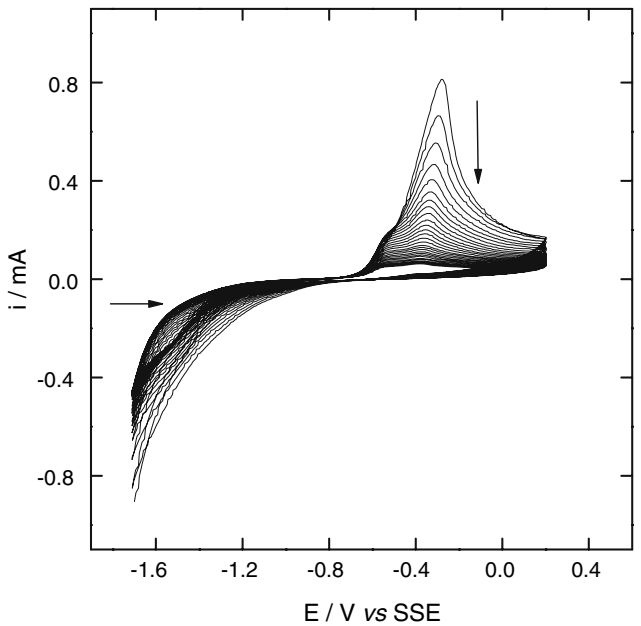

Fig. 2. Successive cyclic voltammograms at 20 mV s^{-1} for a nickel powder randomly dispersed on a graphite + polypropylene matrix in the [−1.7, 0.2] V vs $Hg/HgSO_4/KSO_4$ (sat) potential window. 0.245 M K_2SO_4, 0.005 M H_2SO_4, pH = 2.7, T = 298 K. Deaerated conditions.

The apparent corrosion potential (defined by $i = 0$) measured under such near steady state conditions is $E_{eq} = -0.19$ V vs Ag/AgCl/KCl (sat.). In the cathodic branch of the voltammetric curve, a Tafel region associated with the hydrogen evolution reaction was observed. The measured slope was $b_H = -3\ V^{-1}$. In the anodic branch of the voltammetric curve, a well defined anodic peak was observed at $E_p = -0.005$ V vs Ag/AgCl/KCl (sat.) corresponding to an anodic peak current $i_p = 25\ \mu A$. A Tafel region was also observed and the measured slope in the ascending part of the anodic branch was $b_D = 15\ V^{-1}$. Compared with previously obtained results for nickel powder randomly dispersed in a polymeric matrix [8], this anodic peak is interpreted as corresponding to the active anodic dissolution/passive transition for the nickel component of the electrode material. Similar peaks were also observed for a polycrystalline nickel electrode under the same experimental conditions and interpreted as associated with the active anodic dissolution/passive transition [8, 9, 11].

When successive voltammetric cycles were performed, the observed behaviour of the composite material was very similar to that of a polycrystalline nickel electrode [9–11]. As seen in Figure 2, the peak current values decrease in successive cycles. This can be interpreted as a partial and progressive passivation of the electrode surface [11]. If current peak versus potential peak values were represented in the different cycles, the value of the slope, measured as $\left(dE_p/di_p\right)$, was $R_\Omega = 140\Omega$, which is close to the ohmic drop value measured by means of impedance measurements ($R = 130\Omega$), as discussed in the following section.

For the composite material, measured half peak widths, $\omega_{1/2}$, are higher than the measured ones for the polycrystalline nickel electrode. Moreover, the measured anodic peak potentials are more cathodic than those corresponding to the anodic peak for the polycrystalline nickel electrode (see Table 2). In both cases the slope $\left(d \ln i_p/d \ln v\right)$ (where ν represents the sweep rate) has a value close to 0.5. This indicates that a common rate determining step controls the oxidation process for both a polycrystalline nickel electrode and a nickel powder randomly dispersed in a graphite + polymer composite [9]. The rougher surface of the composite is shown by

Table 2. Voltammetric parameters obtained from the voltammograms recorded at different scan rates. Same experimental conditions as in Figure 2. Symbols: ν, scan rate; E_{eq}: equilibrium potential (defined by $i = 0$); I_{pa}: anodic peak intensity; E_{pa}: anodic peak potential; $\omega_{1/2}$: half width peak; Q_a: anodic charge

Electrode	ν/mV s^{-1}	E_{eq} ($i = 0$)/V	I_{pa}/mA	E_{pa}/V	$\omega_{1/2}$/V	Q_a/mC
Nickel	200	−0.820	6.7	−0.240	0.075	7.0
polycrystalline	150	−0.910	4.7	−0.215	0.100	6.5
	20	−0.680	1.8	−0.295	0.045	9.9
	5	−0.690	1.0	−0.345	0.040	22.0
Composite	200	−1.075	2.3	−0.030	0.225	5.9
	150	−1.060	2.2	−0.050	0.235	7.6
	100	−0.825	1.8	−0.105	0.190	7.4
	80	−0.860	1.6	−0.125	0.200	9.0
	60	−0.790	1.6	−0.150	0.185	11.0
	40	−0.725	1.2	−0.190	0.180	12.0
	20	−0.700	1.1	−0.230	0.160	19.0
	10	−0.695	0.9	−0.260	0.145	30.0
	5	−0.690	0.7	−0.320	0.135	38.0
	1	−0.675	0.4	−0.400	0.100	83.0

the highest calculated charge at a low scan rate, since in this case electrolyte species could be better absorbed in the composite matrix and a greater electroactivity was attained.

Polymer + graphite powder mixtures can be used as electrodes for analytical applications if the conductive load is higher than that required to overcome the first percolation threshold [22, 29]. The graphite powder content (40% in weight) was high enough for such a purpose [29] and electrical conductance of the composite is assured. However, graphite is not a completely inert substance because of the formation of a chemisorbed oxygen layer of carbonyl groups in the presence of molecular oxygen in the media [32]. In fact, a small cathodic peak and a slight shoulder at the beginning of the anodic peak were observed after the first cycle (marked by arrows in Figure 3). These results suggest the existence of a redox process associated to carbonyl groups formed on the surface of the external graphite particles in contact with the solution. This redox process could favour nickel passivation. However, this assumption requires more experimental evidence, since other overlapping processes such as reversible hydrogen evolution are possible in this potential range.

3.3. *Electrochemical Impedance Spectroscopy*

Electrochemical impedance spectra obtained at different stabilization potentials for which an overall anodic current was measured before the peak potential in Figure 1 are represented in Figure 4.

A capacitive tail was observed at low frequencies in Figure 4. This result contrasted with the case of a polycrystalline nickel electrode for which a capacitive loop was observed at low frequencies in the impedance spectra recorded in the electrodissolution potential range [8, 12]. As seen in Figure 4, the capacitive tail tends to fall when the applied stabilization potential becomes more anodic, and finally a pure diffusion component was observed, characterized by a tail with a slope of 45 degrees at low frequencies. This behaviour can be explained by the following simple reaction scheme:

$$\mathrm{Ni} \xrightarrow{k_1} \mathrm{Ni(II)} + 2\mathrm{e}^- \tag{1}$$

$$\mathrm{Ni(II)} \xrightarrow{k_2} \mathrm{Ni}_{\mathrm{aq}}^{2+} \tag{2}$$

Equation (1) represents nickel electrodissolution which forms Ni(II) on the electrode surface, whereas Equation (2) is a simplification of the physico-chemical processes which are associated with the passage of nickel ions to the electrolyte solution [8, 9, 12], such as dissociation and solubilization of Ni (II) species and the transportation of a solvated Ni^{2+} throughout the aqueous media. From a kinetic point of view all these processes are represented by the apparent rate constant k_2. This approximation proved useful in obtaining kinetic information about polycrystalline nickel electrodissolution processes [12]. In the case of a polycrystalline nickel electrode process (2) was favoured by the electrode potential, which indicates a migration component in the associated transportation process [12]. Moreover, the positive charge generated by reaction (2) must be balanced by the anions supplied by the electrolyte which

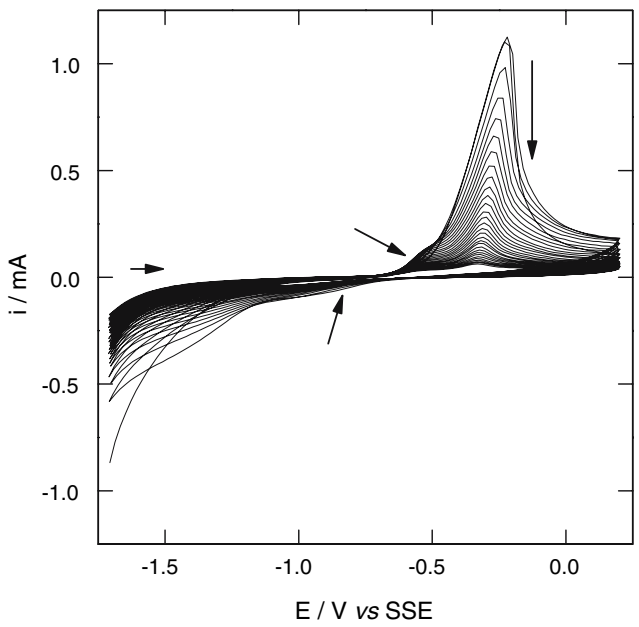

Fig. 3. Successive cyclic voltammograms at 20 mV s^{-1} for a nickel powder randomly dispersed on a graphite + polypropylene matrix in the [−1.7, 0.2] V vs $Hg/HgSO_4/KSO_4$ (sat) potential window. 0.245 M K_2SO_4, 0.005 M H_2SO_4, pH = 2.7, T = 298 K. Aerated conditions (without Ar bubbling).

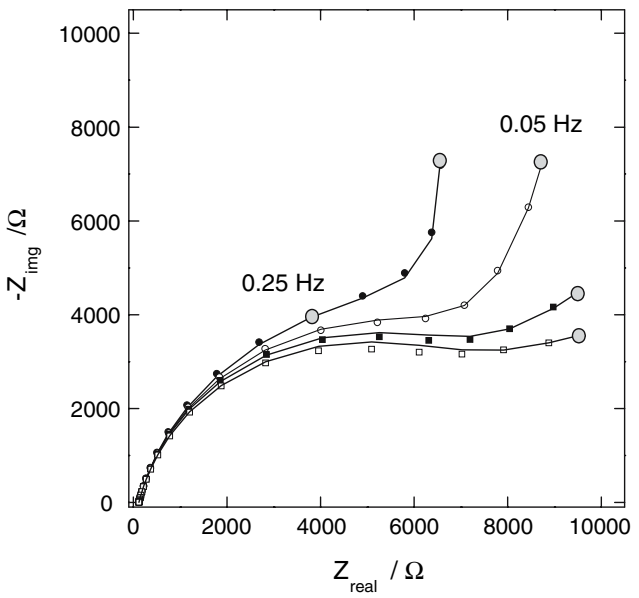

Fig. 4. Electrochemical impedance spectra for the stabilization potentials E_0 = −0.225 V (full circles), E_0 = −0.2 V (open circles), E_0 = −0.175 V (full squares) and E_0 = −0.15 V (open squares). 0.245 M K_2SO_4, 0.005 M H_2SO_4, pH = 2.7, T = 298 K. All the potentials are referred to the Ag/AgCl/KCl (sat.) reference electrode. Solid line indicates the fitting to the considered equivalent circuit.

diffuse towards the electrode surface. As in ref. [12], in the case of a nickel powder randomly dispersed in a graphite + polymer composite, it is considered that k_2 values are potential dependent. If it is considered that initially k_2 has a nearly zero value, then the transport process is barely favoured. Under those conditions, the observed low frequency capacitive tail at $E_0 = -0.225$ V vs Ag/AgCl/KCl (sat.) stabilization potential is related to the capacitance associated with the electrogenerated Ni(II) on the electrode surface. As the stabilization potential (the potential at which each electrochemical impedance spectrum was recorded (see Section 2)) becomes more anodic, the transport process is favoured, and an increasing transport component is observed in the impedance spectra. The fact that a capacitive loop was not observed, as opposed to the case of the polycrystalline nickel [12], may be explained if k_2 values are low at all potentials. The effect of the amount and size of the graphite and nickel particles on k_2 cannot be disregarded, although more experiments are needed in order to gain more insight into this problem.

The experimental electrochemical impedance spectra of Figure 4 have been fitted to the equivalent circuit of Figure 5(a). There is good agreement between the experimental and fitted curves. At the stabilization potential $E_0 = -0.225$ V vs Ag/AgCl/KCl (sat.), the n_2 exponent of the CPE_2 element at low frequencies has a value of 1, consistent with pure capacitive behaviour. n_2 values change from 1 (pure capacitive behaviour) to 0.5 (pure diffusive behaviour) as the stabilization potential becomes more anodic. The values which result from the fitting procedure are represented in Table 3 as a function of the stabilization potential. In all cases the charge transfer resistance R decreases for more anodic

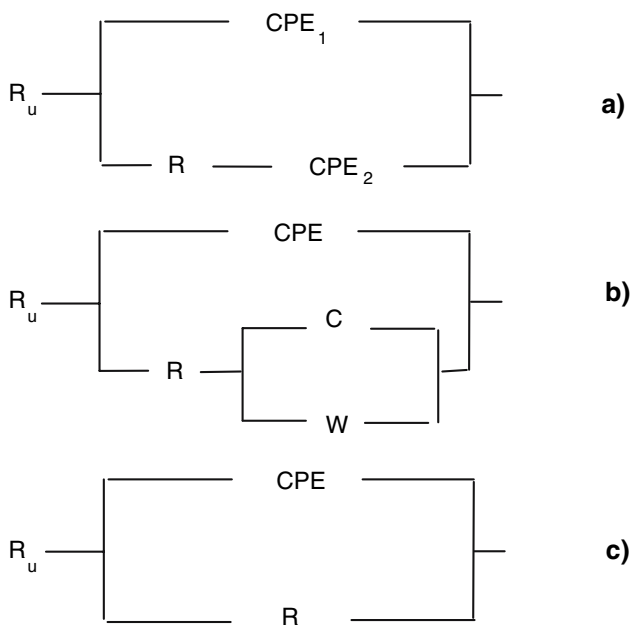

Fig. 5. Different equivalent circuits used in the fitting procedures.

Table 3. Passive elements of the equivalent circuits of Figure 5a and 5b(σ and C) used to fit the measured impedance spectra. $Z_{CPE} = 1/A(j\omega)^n$. In all cases the value for the uncompensated resistance was $R_U = 130\ \Omega$

E/V	A_1/μF s^{n-1}	n_1	R/Ω	A_2/μF s^{n-1}	n_2	σ/Ω s$^{-1/2}$	C/μF
−0.225	41	0.83	10440	190	1	∞	200
−0.200	39	0.84	9460	379	0.88	11520	346
−0.175	39	0.84	8600	534	0.67	2480	347
−0.150	39	0.84	7600	493	0.50	1480	148
−0.125	38	0.84	6700	400	0.45	1500	0
−0.100	37	0.85	6500	298	0.45	1960	0

stabilization potentials as occurs in nickel [8] in this potential range.

The equivalent circuit of Figure 5(b) also reproduces the measured impedance spectra quite well. In this equivalent circuit a C#W arrangement was considered at low frequencies instead of a CPE element. In the equivalent circuit of Figure 5(a), the values for the exponent of the CPE_2 element are lower than 0.85 in several cases (see Table 3). CPE elements are often interpreted as associated with current and potential distributions at the electrode surface and fractal surface morphologies [33, 34]. However, it is very difficult to establish a physical meaning for CPE exponent values lower than 0.85. This is because the equivalent circuit of Figure 5b was used. In this latter circuit C represents the impedance of the capacitance associated with the Ni(II) generated in the electrodissolution process, whereas W represents the impedance associated with the transport process. As the stabilization potential becomes more anodic, the capacitance value C decreases (then, the associated impedance increases as $1/j\omega\ C$) and the Warburg impedance W also decreases (see Table 3), indicating enhanced transport at more anodic stabilization potentials. This result is in agreement with the above qualitative discussion related to the use of the equivalent circuit of Figure 5(a). Thus, the CPE element represents a competitive capacitive/transport component of the impedance associated with the electrochemical process.

In both circuits R is the charge transfer resistance, which is defined by the equation [35]:

$$R = \frac{1}{\left(\frac{\partial i_F}{\partial E}\right)_{ss}} \tag{3}$$

where the subscript ss indicates that the partial derivative is evaluated at each steady state. The following equation is satisfied:

$$Ri_F = \frac{1}{b} \tag{4}$$

where b represents the Tafel constant for the electrodissolution process. This Tafel constant may be obtained form the $\ln(1/R)$ vs E_0 plot as shown in Figure 6 where, in this case, E_0 represents the stabilization potential at which each impedance spectrum was recorded. A value of $b = 4\ V^{-1}$ is obtained, which is lower than that

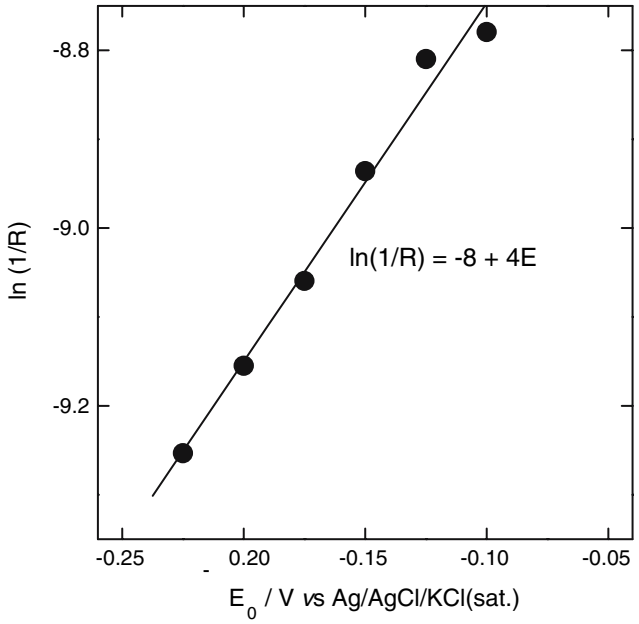

Fig. 6. ln(1/R) vs E_0 plot. R values are determined from the fitting of the impedance spectra of Figure 4 to the equivalent circuit of Figure 5(a).

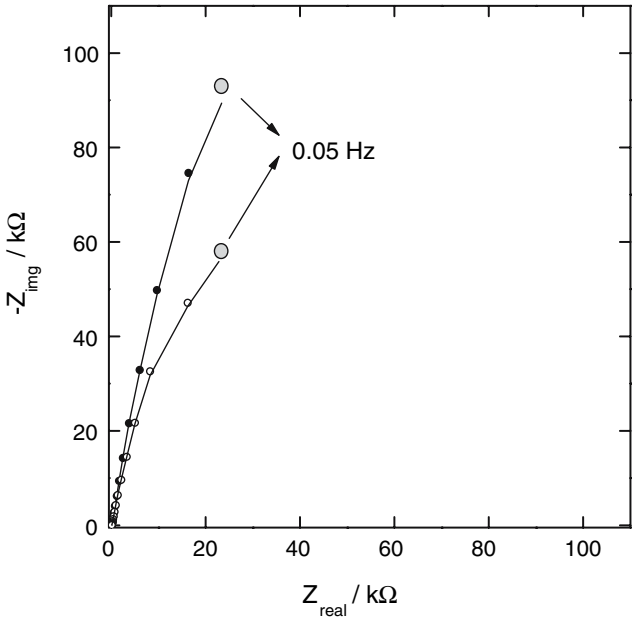

Fig. 7. Electrochemical impedance spectra for the stabilization potentials E_0 = 0.5 V (full circles) and E_0 = 0.8 V (open circles). 0.245 M K_2SO_4, 0.005 M H_2SO_4, pH = 2.7, T = 298 K. All the potentials are referred to the Ag/AgCl/KCl (sat.) reference electrode. Solid line indicates the fitting to the considered equivalent circuit of Figure 5(c).

obtained from low scan rate voltammetric measurements (b_D = 15 V^{-1}). This difference may be related to changes in the rate determining step in the electrodissolution process depending on the perturbation applied to the system [36].

Several of the impedance spectra obtained in the passive potential range are shown in Figure 7.

The measured impedance values were very high, as corresponds to a passive state. The simple equivalent circuit of Figure 5(c) reproduces the experimental results quite well. A CPE element has been considered instead of a pure capacitive element for the high frequency capacitance to improve the fitting. In all analyzed cases the values for the exponent of the CPE element were close to 1 ($n \approx 0.9$) indicating nearly ideal capacitance behaviour. R represents the charge transfer resistance at the metal/passive film interface. Film contributions are not considered here in the equivalent circuit because they are not expected in the frequency interval explored [37]. In Figure 8 the ln($1/R$) vs E_0 plot is shown. Two zones are defined, and after a minimum at approximately 0.4 V vs Ag/AgCl/KCl (sat.), a linear region appears with a slope of 5 V^{-1}. This value is close to that previously obtained in the electrodissolution potential range. If it is considered that the potential drop at the metal/passive film interface is responsible for the charge transfer [38, 39], this result indicates that practically the whole applied potential occurs as a potential drop at the metal/passive film interface under these experimental conditions in the passive potential range. This can be explained by considering the morphological peculiarities of the system. Small islands of electroactive nickel are distributed on the electrode surface and their dielectric properties depend on the applied potential as shown in Figure 9. These islands become passivated in the passive potential range and a non-compact film is electrogenerated. In the case of the polycrystalline nickel electrode the impedance spectra recorded in the passive potential range showed a high frequency capacitive loop associated with the charge transfer at the metal/passive layer interface, followed by a diffusion tail at low frequencies, associated with the

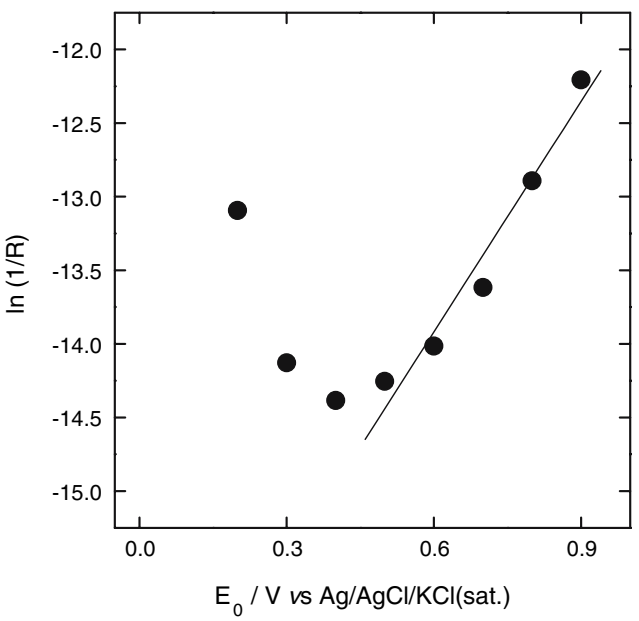

Fig. 8. ln($1/R$) vs E_0 plot. R values are determined from the fitting of the impedance spectra of Figure 7 to the equivalent circuit of Figure 5(c).

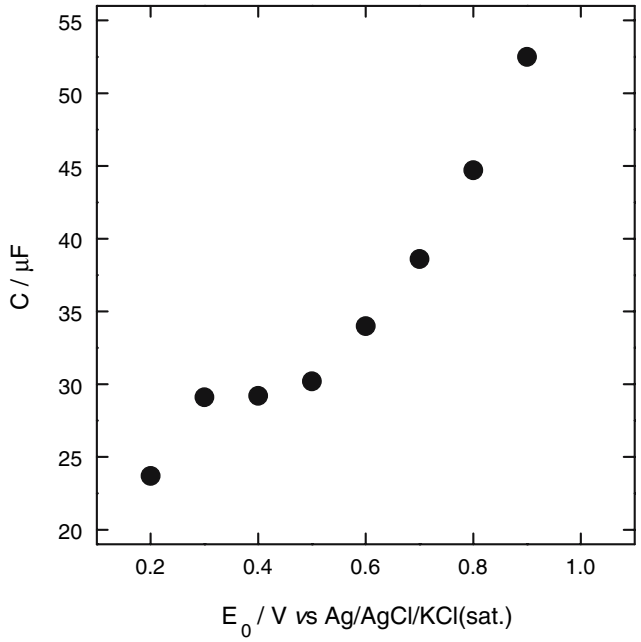

Fig. 9. C vs E_0 plot. C values are determined from A parameter of the CPE which result from the fitting of the impedance spectra of figure 7 to the equivalent circuit of Figure 5(c). In all cases a value close to 0.9 is obtained for the exponent n of the CPE element.

transportation of vacancies within the passive layer [40]. The absence of this diffusion tail in the case of the composite electrode is an indication of a non-uniform passive layer.

4. Conclusions

Under voltammetric conditions the electrodissolution behaviour of an electrode made from a nickel powder randomly dispersed in a graphite + polyethylene matrix is similar to the electrodissolution behaviour of a polycrystalline nickel electrode. Differences between their respective voltammograms may be attributed to the uncompensated resistance and also to the rougher morphology of the composite material.

Under EIS measurement conditions, the electrodissolution behaviour of the nickel powder randomly dispersed on a graphite + polypropylene matrix is partially limited by the diffusion of the anions in the electrolyte in order to electroneutralize the excess of electrogenerated positive charge. The low frequency range of the measured impedance spectra can be interpreted as a parallel arrangement of a capacitive and a Warburg impedance, instead of a CPE element. Moreover, the Tafel constant measured under EIS conditions is lower than that measured in low scan voltammetry, in contrast to the observed behaviour for a polycrystalline nickel electrode. The rate determining step under EIS conditions for nickel electrodissolution is different in the two cases. This result is in agreement with the diffusion limiting electrodissolution for the composite electrode, since this diffusion limitation is not observed for a polycrystalline nickel.

Acknowledgements

This work was supported by the Spanish Ministry of Science and Technology (Project CICyT-CTQ2004-08026/BQU) and Spanish Ministry of Environmental (Project 6.1-210/2005). J. Gregori acknowledges a Fellowship from the Spanish Education Ministery (FPU program). J.J. García-Jareño acknowledges the Spanish Ministry of Science and Technology for their position (''Ramón y Cajal'' Program). The authors would like to express our gratitude for the valuable and interesting comments of Professor A.A. Wragg about this work.

References

1. S.G. Kim, S.P. Yoon, J. Han, S.W. Nam, T.H. Lim, I.H. Oh and S.A. Hong, *Electrochim. Acta* **49** (2004) 3081.
2. V. Rashkova, S. Kitova, I. Konstantinov and T. Vitanov, *Electrochim. Acta* **47** (2002) 1555.
3. X. Wang, H. Luo, H. Yang, P.J. Sebastián and S.A. Gamboa, *Int. J. Hydrogen Energy* **29** (2004) 967.
4. E.M.A. Martini, S.T. Amaral and I.L. Müller, *Corros. Sci.* **46** (2004) 2097.
5. P. Marcus, *Electrochim. Acta* **43** (1998) 109.
6. A. Gildenpfennig, U. Gramberg and G. Hohlneicher, *Corros. Sci.* **45** (2003) 575.
7. A. Jouanneau, M. Keddam and M.C. Petit, *Electrochim. Acta* **21** (1976) 287.
8. M.R. Barbosa, J.A. Bastos, J.J. Gacía-Jareño and F. Vicente, *Electrochim. Acta* **44** (1998) 957.
9. M.R. Barbosa, S.G. Real, J.R. Vilche and A.J. Arvía, *J. Electrochem. Soc.* **135** (1988) 1077.
10. S.G. Real, M.R. Barbosa, J.R. Vilche and A.J. Arvía, *J. Electrochem. Soc.* **137** (1990) 1696.
11. J. Gregori, J. Agrisuelas, D. Giménez, M.P. Peña, J.J. García-Jareño and F. Vicente, *Rev. Metal.* **39** (2003) 346.
12. J. Gregori, J.J. García-Jareño, D. Giménez and F. Vicente, *J. Solid State Electr.* **9** (2005) 83.
13. J. Delmonte, *Metal-Polymer Composites* (Van Nostrand Reinhold, New York, 1990), pp. 163.
14. H.S. Katz and J.V. Milewski, *Handbook of Fillers for Plastics* (Van Nostrand Reinhold, New York, 1987), pp. 20.
15. J.T. Long and S.G. Weber, *Anal. Chem.* **60** (1988) 2309.
16. K.M. Korfhage, K. Ravichandran and R.P. Baldwin, *Anal. Chem.* **56** (1984) 1514.
17. D.E. Tallman and S.L. Petersen, *Electroanalysis* **2** (1990) 499.
18. A. Dailly, J. Ghanbaja, P. Willmann and D. Billaud, *J. Appl. Electrochem.* **34** (2004) 885.
19. B. Jugovic, J. Stevanovic and M. Marksimovic, *J. Appl. Electrochem.* **34** (2004) 175.
20. J.N. Balaraju, T.S.N.S. Narayanan and S.K. Seshadri, *J. Appl. Electrochem.* **33** (2003) 807.
21. J. Navarro-Laboulais, J. Trijueque, J.J. García-Jareño, D. Benito and F. Vicente, *J. Electroanal. Chem.* **444** (1998) 173.
22. J. Trijueque, J.J. García-Jareño, J. Navarro-Laboulais, A. Sanmatías and F. Vicente, *Electrochim. Acta* **45** (1999) 789.
23. A. Sanmatías, D. Benito, J.A. Bastos, J. Navarro-Laboulais, J.J. García-Jareño and F. Vicente, *Int. J. Inorg. Mater. (Solid State Sci.)* **1** (1999) 361.

24. A. Sanmatías, D. Benito, J.A. Bastos, J.J. García-Jareño and F. Vicente, *Int. J. Inorg. Mater. (Solid State Sci.)* **1** (1999) 373–378.
25. J. Navarro-Laboulais, J. López, X. Villanueva, Benito, J.J. García-Jareño and F. Vicente, *J. Electroanal. Chem.* **484** (2000) 33.
26. J. Navarro-Laboulais, J.J. García-Jareño and F. Vicente, *J. Electroanal. Chem.* **536** (2002) 11.
27. L. Beaunier, M. Keddam, J.J. García-Jareño, F. Vicente and J. Navarro-Laboulais, *J. Electroanal. Chem.* **566** (2004) 159.
28. J.R. Macdonald, *Solid State Ionics* **58** (1992) 97.
29. J. Navarro-Laboulais, J. Trijueque, F. Vicente and H. Scholl, *J. Electroanal. Chem.* **379** (1994) 159.
30. J. Navarro-Loboulais, J. Trijueque, J.J. Garcia-Jareño and F. Vicente, *J. Electroanal. Chem.* **399** (1995) 115.
31. J. Navarro-Laboulais, J. Trijueque, J.J. Garcia-Jareño and F. Vicente, *J. Electroanal. Chem.* **422** (1997) 91.
32. T.G. Ros, A.J. van Dillen, J.W. Geus and D.C. Koningsberger, *Chem.-Eur. J.* **8** (2002) 1151.
33. Z. Kerner and T. Pajkossy, *J. Electroanal. Chem.* **448** (1998) 139.
34. Z. Kerner and T. Pajkossy, *Electrochim. Acta* **46** (1998) 207.
35. M. Keddam, O.R. Mattos and H. Takenouti, *J. Electrochem. Soc.* **128** (1981) 257.
36. N. Sato and G. Okamoto, *J. Electrochem. Soc.* **111** (1964) 897.
37. C. Clerc and D. Landolt, *Electrochim. Acta* **33** (1988) 859.
38. C.V. D'Alkaine and M.A. Santanna, *J. Electroanal. Chem.* **457** (1998) 13.
39. D.D. Macdonald, S.R. Biaggio and H. Song, *J. Electrochem. Soc.* **139** (1992) 170.
40. D.D. Macdonald, R.Y. Liang and B.G. Pound, *J. Electrochem. Soc.* **12** (1987) 134.